Carbonation by fluid–rock interactions at high-pressure conditions: Implications for carbon cycling in subduction zones

Francesca Piccoli, Alberto Vitale Brovarone, Olivier Beyssac, Isabelle Martinez, Jay J. Ague, Carine Chaduteau

Carbonation by fluid-rock interactions at High-Pressure conditions: implications for carbon cycling in subduction zones

Francesca Piccoli[a,*], Alberto Vitale Brovarone[a], Olivier Beyssac[a], Isabelle Martinez[b], Jay J. Ague[c,d], Carine Chaduteau[b]

[a]Insitut de Minéralogie, Physique des Matériaux et Cosmochimie (IMPMC), UPMC-CNRS Campus Jussieu, case courrier 115, 4 Place Jussieu, 75005, Paris, France. Tel. 0033 (0)1 44 27 25 60

[b]Institut de Physique du Globe de Paris, Sorbonne Paris Cité, Université Paris Diderot, UMR 7154 CNRS, 1 rue Jussieu, F-75005 Paris, France

[c]Department of Geology and Geophysics, Yale University, P.O. Box 208109, New Haven, CT 06520-8109, USA

[d]Peabody Museum of Natural History, Yale University, 170 Whitney Avenue, P.O. Box 208118, New Haven, CT, 06520-8118, USA

*francesca.piccoli@impmc.upmc.fr

Abstract

Carbonate-bearing lithologies are the main carbon carrier into subduction zones. Their evolution during metamorphism largely controls the fate of carbon, regulating its fluxes between shallow and deep reservoirs. Recent estimates predict that almost all subducted carbon is transferred into the crust and lithospheric mantle during subduction metamorphism via decarbonation and dissolution reactions at high-pressure conditions. Here we report the occurrence of eclogite-facies marbles associated with metasomatic systems in Alpine Corsica (France). The occurrence of these marbles along major fluid-conduits as well as textural, geochemical and isotopic data indicating fluid-mineral reactions are compelling evidence for the precipitation of these carbonate-rich assemblages from carbonic fluids during metamorphism. The discovery of metasomatic marbles brings new insights into the fate of carbonic fluids formed in subducting slabs. We infer that rock carbonation can occur at high-pressure conditions by either vein-injection or chemical replacement mechanisms. This indicates that carbonic fluids produced by decarbonation reactions and carbonate dissolution may not be directly transferred to the mantle wedge, but can interact with slab and mantle-forming rocks. Rock-carbonation by fluid-rock interactions may have an important impact on the residence time of carbon and oxygen in subduction zones and lithospheric mantle reservoirs as well as carbonate isotopic signatures in subduction zones. Furthermore, carbonation may modulate the emission of CO_2 at volcanic arcs over geological time scales.

Keywords: Subduction carbon cycle, Carbonation, CO_2 sequestration, Metasomatism

1. Introduction

Subduction exerts a key role in the long-term carbon cycle by regulating the fluxes of carbon between the Earth's surface and the deep Earth. The redistribution of carbon between the exogenic and endogenic reservoirs largely depends on the evolution of carbonate-bearing lithologies in subduction zones. Carbonates are present in sedimentary, mafic and ultramafic lithologies, and constitute the dominant reservoir of carbon in the subducting lithosphere (Alt and Teagle, 1999; Kelemen & Manning, 2015). There is growing evidence that carbonates can be extremely reactive during subduction metamorphism via devolatilization reactions (Cook-Kollars et al., 2014; Kerrick & Connolly, 2001), as well as carbonate dissolution via fluid-rock interactions at high-pressure conditions (Frezzotti et al., 2011; Ague and Nicolescu, 2014; Kelemen and Manning, 2015), carbonate reduction reactions (Galvez et al., 2013a; Malvoisin et al., 2012), or melting of the subducting crust (Poli, 2015). Nonetheless, key questions remain regarding the mechanisms of carbonic fluid transfer from the slab to the lithospheric mantle in the sub-arc region, their role in mantle wedge metasomatism, and their contribution to the CO_2 degassing at volcanic arcs.

To address these questions, a growing number of studies have been carried out using both experimental petrology (Molina and Poli 2000; Poli et al., 2009) and thermodynamic modeling (Kerrick and Connolly 2001; Gorman et al., 2006). All these studies agree that, considering a "closed system" (no external fluid supply), significant carbon transfer to the mantle wedge is feasible only at shallow depth in the forearc region. This transfer is made possible via devolatilization reactions that, based on experimental and thermodynamic results, are much more limited at deeper, subarc conditions (Connolly, 2005; Poli et al., 2009). Nevertheless, the role of fluid-rock interactions appears to be critical for the stability of carbonates. Recently, field based studies (Ague and Nicolescu, 2014; Frezzotti et al., 2011) as well as theoretical and experimental works (Facq et al., 2014; Sverjensky et al., 2014) have pointed out that massive carbonate dissolution in fluids may occur at high-pressure-low

87 temperature conditions and can generate large amounts of carbonic fluids (see Kelemen and
88 Manning, 2015 for review). Accounting for carbonate dissolution at high-pressure conditions
89 in comprehensive budgets overturns older paradigms on carbonate stability with respect to
90 carbon mobility in subduction zones. The most recent budgets actually predict that carbonate
91 dissolution allows almost all subducted carbon to be transferred to the mantle wedge
92 (Kelemen & Manning, 2015). Owing to the very recent discovery of these processes, much
93 remains to be learned about the fate of these carbonic fluids and their interaction with slab-
94 and mantle-forming rocks.

95 Here, we report the occurrence of eclogite-facies marbles formed by fluid-rock
96 interaction processes (metasomatism) occurring along intensely metasomatized lithological
97 interfaces (Alpine Corsica, France). We present and discuss the occurrence, textures,
98 mineralogy and geochemistry of these metasomatic marbles. We then propose a mechanism
99 of carbonates formation by precipitation and mineral carbonation by carbonic fluid-rock
100 interactions at high-pressure conditions. Finally, the implications and contribution of rock
101 carbonation to the deep carbon fluxes and cycling are discussed.

102

103 **2. Geological setting**

104 Alpine Corsica (France) is a branch of the Alpine orogenic system (Jolivet et al., 1991; Molli
105 and Malavieille, 2011) (Fig.1a). The belt mainly includes remnants of subducted Mesozoic
106 slow-spreading oceanic and passive margin lithosphere, which formed part of the Tethys
107 Ocean basin. This rock package is classically referred to as the Schistes Lustrés Complex
108 (Fig. 1b; Jolivet et al., 1990; Fournier et al., 1991; Malavieille et al., 1998; Vitale Brovarone
109 et al., 2013). The exceptional preservation of prograde-to-peak mineral assemblages,
110 including widespread lawsonite, makes the Schistes Lustrés of Alpine Corsica an excellent

111 site for field investigations related to subduction. These units underwent various metamorphic
112 overprints during the Alpine subduction ranging from subgreenschist-facies conditions of
113 about 300°C and 0.5 GPa to lawsonite blueschist and lawsonite eclogite-facies conditions
114 which reached 500-550 °C and ~2.3 GPa (e.g. Fournier et al., 1991; see Vitale Brovarone et
115 al., 2013 for review).

116 Carbonate-bearing rocks are widespread in the Schistes Lustrés of Alpine Corsica. The
117 most typical carbonate-bearing lithologies are metamorphosed oceanic sediments (referred to
118 as calcschists hereafter), ophicarbonate, and carbonated metabasalts (Miller et al., 2001;
119 Ravna et al., 2010; Vitale Brovarone et al., 2011b). In each lithology, primary carbonates and
120 various generations of carbonate veins are observed (Miller et al., 2001; Ravna et al., 2010;
121 Vitale Brovarone et al., 2011b). These veins have been shown to be in most cases in isotopic
122 equilibrium with the host rocks with little effect of external fluid infiltrations and
123 metasomatism (Cartwright and Buick, 2000). On the other hand, evidence for high-pressure-
124 low temperature fluid-rock interactions and metasomatism in the Schistes Lustrés of Alpine
125 Corsica is widespread, most typically localized at lithological interfaces. In this work, we
126 focus on processes occurring where serpentinites are in contact with metasedimentary rocks.

127 Here, past results on high-pressure metasomatism in Alpine Corsica are briefly
128 summarized. In the blueschist-facies zone, reactions between serpentinites and overlying
129 metasediments led to carbonate reduction and precipitation of wollastonite and abiotic
130 graphite at blueschist-facies conditions (Malvoisin et al., 2012; Galvez et al., 2013a). Except
131 for the influx of external, serpentinite-derived fluids, the reacted metasediments revealed
132 largely conservative carbon budget (Galvez et al., 2013a). In similar lithological settings,
133 massive precipitation of lawsonite from fluid-rock interactions at the expense of
134 metasedimentary rocks in contact with serpentinites testifies to the reincorporation of large
135 amounts of water in the rock at prograde blueschist-to-eclogite-facies metamorphic conditions

(Martin et al., 2011; Vitale Brovarone et al., 2014; Vitale Brovarone and Beyssac, 2014;). This process is characterized by a dramatic whole-rock chemical modification leading to mafic/ultramafic, Ca-rich metasomatic products.

The carbonate-rich rocks studied herein are intimately related to the latter Ca-rich metasomatic rocks and were collected in the lawsonite eclogite-facies San Petrone unit. This unit is characterized by a basal body of serpentinite variably overlain by Jurassic pillow metabasalts, Mesozoic metasediments (e.g. calcschists, marbles, Mn-metacherts) or slivers of Hercynian continental basement rocks mainly consisting of pre-Alpine, carbonate-free, high-temperature metasediments and granitic rocks overprinted at high-pressure-low temperature conditions during the Alpine subduction (Vitale Brovarone et al., 2011b; Fig. 1c). Ophicarbonate rocks are locally found at the top of the serpentinite body. The San Petrone unit has been considered as a remnant of a Mesozoic hyper-extended passive margin (Vitale Brovarone et al., 2011b; Beltrando et al., 2014). Peak metamorphic conditions in this unit are estimated at ca. 490-530 °C and ~2.3 GPa by means of pseudosection modeling and thermometry based on Raman spectroscopy of carbonaceous material (Ravna et al., 2010; Vitale Brovarone et al., 2011a, 2013). The peak metamorphic age of ~34 Ma has been determined by several techniques including U-Pb zircon and Lu-Hf garnet and lawsonite geochronology (Martin et al., 2011; Vitale Brovarone and Herwartz, 2013).

3. Structural occurrence of metasomatic marbles

The carbonate-rich rocks which are the subject of this paper occur along a regional lithological boundary separating serpentinites from either slivers of Hercynian basement rocks (dominantly pre-Alpine high temperature metasedimentary rocks) or Mesozoic metasedimentary rocks (Figs. 1c and 2). The first few meters of rock above the serpentinites

exhibit intense Alpine metasomatism that has already been described in previous studies (Martin et al., 2011; Vitale Brovarone et al., 2011b, 2014). These metasomatic rinds can be followed for several kilometers along the top of the serpentinite body and are characterized by lawsonite-rich assemblages, but diopside-rich rocks are also common. These rocks are referred to as Stage#1 diopside-lawsonite rocks (Fig.2). The carbonated rocks which are the subject of this study are referred to as Stage#2 metasomatic marbles (or simply metasomatic marbles), these form discontinuous patches or lenses of variable thickness and lateral extension (from a few tens of cm to several m, Fig. 2), and are preferentially associated with diopside-rich rather than the lawsonite-rich metasomatic rocks. The petrological differences between Stage#2 metasomatic marbles and Mesozoic metasediments are discussed in Section 5.

The metasomatic marbles show a range of structural relationships with the surrounding diopside-lawsonite rocks, and the carbonate/host rock ratios are extremely variable. Figure 2 summarizes the field relationships between the different rock types, i.e. serpentinites, Stage#1 diopside-lawsonite rocks, Stage#2 metasomatic marbles, and the inferred protolith rocks (continental basement rocks or Mesozoic metasediments). The transition from diopside-lawsonite rocks to Stage#2 metasomatic marbles is marked by a gradual increase of carbonate/host rock ratio, passing from diopside-lawsonite rocks to isolated carbonate-rich veins in Stage#1 host rocks, to Stage#2 metasomatic marbles with remnants of Stage#1 rocks. Isolated veins have crack-seal texture and are mainly composed of rod-shaped Ca-carbonate ± omphacite (Figs. 3a, b, d). Carbonate rods are perpendicular to the vein walls (Fig. 3b). Omphacite grows from the vein wall toward the center (Fig. 3d). Some veins exhibit interaction with the host Stage#1 rocks characterized by omphacite replacement of the precursor diopside (Al-Na gain; Ca-Mg loss) and local carbonate precipitation (Fig. 3d). The abundance of omphacite decreases from the vein wall to the host rock. Diopside far from the

vein does not display any chemical zoning involving Na-Al enrichment. The isolated veins are connected to dm-thick layers (ca. 20 cm) showing similar crack-seal textures (Figs. 2 and 3a). These layers are meter-scale and are parallel to the wallrock foliation (Fig. 2). Outcrop-scale hydraulic breccias consisting of cm- to m-scale angular clasts of Stage#1 diopside-lawsonite rocks embedded within a carbonate vein network provide strong evidence for diffuse hydrofracturing and carbonate precipitation (Figs. 2, 3e and f).

In some outcrops, serpentinites are overlain by a sequence of metasomatic marbles ranging in thickness from less than one m to ~10m (Figs. 2, 3g and 4a). These metasomatic marbles are hosted within the diopside-lawsonite rock and contain remnants of the host rock—ranging from a few microns to several centimeters—floating in a carbonate-dominated matrix. Remnants of diopside-lawsonite rocks in the metasomatic marbles differ from the angular clasts found in the hydraulic breccias. First, they have embayed margins and microtextures (see Section 5) suggest digestion of the silicate portions into the carbonate matrix. Second, the host rock remnants preserve their original orientation (Fig. 4a), whereas the clasts in the hydraulic breccias have random rotation (Figs. 2). Last, the diopside remnants are commonly rimmed by omphacite, the latter being in textural equilibrium with the carbonate as observed in the isolated carbonate veins.

4. Methods

4.1 Scanning electron microscopy and electron microprobe

Petrographic thin sections were carbon coated for scanning electron microscopy (SEM). Observations were performed at a working distance of 7.5 mm using a Zeiss Ultra 55 field emission gun SEM operated at 15 kV with a 120 μm aperture. Backscattered electron (BSE) mode was used to investigate chemical heterogeneities using an Angle Selective

209 Backscattered Detector (AsB) or an Energy Selective Backscattered Detector (EsB). Energy
210 dispersive X-ray spectrometry (EDXS) maps were acquired using an EDXS QUANTAX
211 system equipped with a silicon drift detector XFlash 4010 (Bruker). Data were processed with
212 the software Esprit (Bruker). Mineral analyses were performed on a Cameca electron
213 microprobe (either SX-100 or SX Five) (Camparis, Université Paris 6). Common analytical
214 conditions were adopted for spot analyses [15 kV, 10 nA, wavelength-dispersive spectroscopy
215 (WDS) mode], using Fe_2O_3, $MnTiO_3$ (Mn, Ti), diopside (Mg, Si), orthoclase (Al, K),
216 anorthite (Ca) and albite (Na) as standards. The automated Cameca ZAF procedure was used
217 for quantification (Tables S1, S2, S4 and S5).

218 *4.2 Whole rock major and trace element data*

219 Chips of low to highly carbonated rock were removed from hand-samples. Samples were
220 crushed in an agate mortar (grain size < 80μm) and sent for major and trace element, CO_2 and
221 organic carbon analyses at the Service d'Analyse des Roches et Minéraux (SARM, Centre de
222 Recherches Pétrographiques et Géochimiques, Nancy, France) by alkali fusion of rock
223 samples ($LiBO_2$), followed by concentration measurements using an ICP-OES Icap 6500
224 (Thermoscientific) for major elements, and an ICP-MS X7 (Thermoscientific) for minor
225 elements (protocol by Carignan et al., 2001). The modal proportions of silicates vs. carbonate
226 were estimated first with optical microscopy and then checked using whole rock and mineral
227 composition. In two cases, samples 1COR12-20d and COR13-29c, two different chips were
228 taken: one representative of the metasomatic marble, where silicates are present as clasts, and
229 another one representative of a Stage#1 diopside+lawsonite rock, where carbonate is a minor
230 constituent. When an average value is indicated, the standard deviation (1σ) is also reported
231 (Tables 1 and S2).

232 *4.3 Carbon mass balance calculation*

In/out carbon fluxes in the subducting slab (during high-pressure metamorphism) are estimated from the grams of CO_2 per 100g of rock released by decarbonation reaction and carbonate dissolution vs. the grams of CO_2 per 100g of rock bound by rock carbonation process (Section 8.3). The CO_2 bound in the rocks of this study was back calculated from whole rock analyses removing the measured organic carbon content to the measured CO_2 (red bar in Fig. 8a, see also Table S2). Values for CO_2 released per 100g of rock after carbonate dissolution (Ague and Nicolescu, 2014) and decarbonation of calcschists (Cook-Kollars et al., 2014) are taken from the literature. For the data on carbonate dissolution (Ague and Nicolescu, 2014), we took the average of the estimated CO_2 loss in samples from Syros (35.1g) and Tinos (22.2g), thus resulting in 28.65 g of CO_2 lost during carbonate dissolution (blue bar in Fig. 8a). For samples affected by decarbonation, we took the calcschist modeled by Cook-Kollars et al. (2014). This rock initially contains 40 wt.% carbonate (i.e. the initial CO_2 content is 17.6g per 100 of rock) and it loses 50% of its initial CO_2, thus 8.8g per 100g of rock (green bar in Fig. 8a). Cook-Kollars et al. (2014) highlighted that natural samples from Schist Lustrés and Cignana suite show a lower extent of decarbonation. They conclude that decarbonation reactions during metamorphism may cause the loss of 10 to 20% of the initial CO_2. We took the intermediate value of 15%. Thus, considering the same initial CO_2 content of 17.6g per 100 g of precursor rock, the CO_2 lost is 2.64g per 100g of rock (orange bar in Fig. 8a).

4.4 Stable isotope data

4.4.1 Carbon and Oxygen isotopes of calcite

Chips of carbonate were taken from hand-samples and crushed in an agate mortar. Raman and SEM analyses establish that the carbonate is nearly pure Ca-carbonate. The isotopic composition of calcite was measured by an AP2003 continuous flow mass spectrometer at

LGIS, IPGP. Approximately 2 to 2.5 mg of sample were loaded in vials; three standards of pure calcite were also used for calibration of both concentration and isotopic composition. After flushing with ultrapure helium, orthophosphoric acid (H_3PO_4) was introduced in each tube in order to produce gaseous CO_2. After 4 hours of reaction at ambient temperature, calcite completely decomposes to release CO_2 (McCrea, 1950); gases were then transferred into the mass spectrometer for analysis. In order to improve the precision of the measurements, each analysis was repeated four times for each vial, and each sample analysed twice. The isotopic $^{13}C/^{12}C$ and $^{18}O/^{16}O$ ratios are expressed using the conventional δ-notation relative to PDB and SMOW international standards. The precision is 0.1‰ for $\delta^{13}C$ and 0.2‰ for $\delta^{18}O$. The results are reported in Table S3. When an average value is indicated, the standard deviation (1σ) is also reported.

4.4.2 Oxygen isotopes of clinopyroxene

A polished sample of omphacite+carbonate vein hosted in diopside-lawsonite rock was first studied by SEM to identify zones representative of Stage#1 diopside and Stage#2 omphacite (Figs. 3d and S2). Aliquots of carbonate+omphacite vein were crushed (<100 μm) and single crystals of omphacite were separated by handpicking under a binocular microscope. Diopside-rich protolith rock was sampled out of the vein selvage (ca. 2 cm from the vein) in order to avoid the isotopic contribution of the vein-related omphacite rims, as checked by SEM. Rock was crushed (<100 μm) and single crystals of diopside were separated by handpicking under a binocular microscope. Approximately 2 mg of omphacite and 2 mg of diopside were analyzed using laser fluorination at IPGP (Paris, France) along with UWG-2 garnet standard. Analytical methods are similar to those documented in Rumble et al. (1997). The oxygen isotopic ratios are reported using the international V-SMOW standard. Measurement of UWG-2 garnet standard aliquots gave 2σ external error on $\delta^{18}O$ of ±0.036‰, which is in the

281 same range of in-run uncertainties for individual measurements (<0.03‰). Measurements
282 were duplicated for omphacite, while for diopside the material collected was not sufficient.
283 Fractionation factors (Hoffbauer et al., 1994) were used to infer oxygen isotopes equilibrium
284 temperature between carbonate and clinopyroxenes (Table S3.1). Estimated errors using a
285 Monte Carlo simulation on the calculated temperatures are 30°C and 20°C for the omphacite-
286 calcite and diopside-calcite equilibrium, respectively.

287

288 **5. Petrography of selected metasomatic marbles**

289 Metasomatic marbles have characteristic features that make them different from any other
290 carbonate-bearing rocks of the Schistes Lustrés (i.e. Mesozoic impure marbles, calcschists
291 and ophicarbonates), although they may display mineralogical and chemical variations from
292 one to another outcrop. As an example, the matrix carbonate in these rocks systematically
293 displays a rod-shaped habit with rods oriented at high angles to the regional schistosity or to
294 the margin of Stage#1 clasts in hydraulic breccias (Fig. 3b). In all but one metasomatic
295 marble, the carbonate is a Ca-carbonate phase. Matrix carbonate is calcite, whereas aragonite
296 was found as inclusions in garnet and apatite (see Fig. S1). Dolomite was detected in only one
297 sample by Raman spectroscopy and it was in very small proportions compared to Ca-
298 carbonate (dolomite content below X-ray diffraction detection limit). No ankerite was
299 observed in these rocks, whereas it is common in calcschists and ophicarbonates of the
300 Schistes Lustrés. As Ca-carbonate is the dominant carbonate phase, we will use hereafter the
301 term "carbonate" to indicate compositionally pure Ca-carbonate (i.e. calcite after aragonite).

302 In thin section, metasomatic marbles display a characteristic structure defined by carbonate-
303 rich and diopside-lawsonite-rich domains, the latter occurring as either continuous layers or
304 isolated patches (Figs. 4b, d, e). A compositional layering is defined by the alternation of

carbonate aggregates with diopside (±lawsonite) aggregates. Calcite rods are mm-sized; diopside and lawsonite grain size ranges from μm to mm. The mineral assemblage most commonly consists of carbonate, diopside and lawsonite, with modal proportions varying from sample to sample (Fig. 4). Garnet is also present in several samples. It is found as euhedral, μm to mm-sized crystals in textural equilibrium with carbonate. Its composition ranges from grossular to almandine-spessartine solid solution (Table S4). Phengite, epidote, quartz and pumpellyite (Table S5) are also present. Common accessory phases are titanite, apatite and graphite. Although such assemblages are described in calcschists in the Western Alps (see e.g. Cook-Kollars et al., 2014), they have never been documented in Alpine Corsica to our knowledge. Moreover, the textural and mineralogical features of these silicates indicate that they resulted from intense metasomatism during their high-pressure evolution, as described below.

For simplicity, two dominant mineralogical assemblages representative of Stage#1 and Stage#2 rocks are distinguished, i.e. diopside + lawsonite and carbonate + omphacite, respectively. As mentioned above, additional phases may be present from one sample to another. The chronological relations between the two mineralogical assemblages may be deciphered from the outcrop-scale down to the micro-scale. Diopside ($Quadrilateral_{96.5}$ $Aegirine_{3.5}$; classification after Morimoto, 1989; see Tab. S1) formation at high-pressure conditions during subduction is demonstrated by: (i) the occurrence of diopside veins cross-cutting lawsonite-bearing fabrics (Fig. 3d) and (ii) the fact that the diopside veins are in turn cut by carbonate+omphacite veins, indicating near peak P-T metamorphic conditions. In the carbonate-bearing domains, diopside in contact with carbonate shows either embayed grain boundaries or newly-formed compositional coronas of omphacite (Figs. 5a; $Jadeite_{39.5}$ $Quadrilateral_{44.5}$ $Aegirine_{16}$; see Tab. S1). Tiny (c.a. 10-20 μm), second generation idioblastic lawsonite crystals were locally found in the carbonate. In the vein selvage, omphacite rims on

330 diopside (Fig. 5b) have the same composition as omphacite growing together with carbonate
331 in the vein. In metasomatic marbles, atoll-like textures show relict diopside cores being
332 replaced by carbonate and rimmed by omphacite (Fig. 5a), the latter being in textural
333 equilibrium with the carbonate matrix. The abundance of omphacite varies from one sample
334 to another. All transitional stages from carbonate-free diopside-lawsonite rocks to carbonate-
335 rich rocks are depicted in Figure 4.

336 Only one sample (COR13-21d) displays a different mineralogy, composed of (in order of
337 volume abundance): calcite, actinolite, chlorite and clinopyroxene. This sample was collected
338 within a sequence of typical metasomatic marbles, and shares with them similar characteristic
339 features such as rod-shaped carbonate and Na-rich clinopyroxene coronas (aegirine-augite,
340 Na-Fe^{3+} rich clinopyroxene, see Fig. 5c) on relict diopside. Geochemical data for this sample
341 are given in Section 6.

342

343 **6. Whole rock chemical compositions**

344 Samples of metasomatic marbles were analyzed for their major and trace element bulk
345 composition (Table S2). Reference samples of Mesozoic calcschist and ophicarbonate
346 unaffected by metasomatism (i.e. far from the studied lithological boundaries and showing no
347 mineralogical or textural evidence for fluid-rock interactions), were also analyzed (Table S2).
348 Table 1 reports the average major element composition of metasomatic marble as well as the
349 compositions of a Stage#1 diopside-lawsonite rock (sample OF3598 in Vitale Brovarone et
350 al., 2014) and a Stage#1 rock with higher lawsonite content (lawsonite mode c.a. 75%;
351 sample COE5, Martin et al., 2011).

352 The variability of both Stage#1 rocks and Stage#2 metasomatic marbles hampers
353 quantitative mass balance calculation. Here, only concentrations of the most representative

354 oxides CaO, MgO, SiO_2 and CO_2 are presented. Metasomatic marbles have variable
355 compositions based on the carbonate-silicate modal proportions (Tables 1, S2). The average
356 composition is: CaO 39 wt.% (±5%, 1σ); CO_2 27 wt.% (±6%, 1σ); SiO_2 20 wt.% (±6%, 1σ)
357 and MgO 3 wt.% (±2%, 1σ). The silicate mode in sample COR13-21d is higher, thus
358 resulting in a slightly different bulk rock composition (CaO 22%; CO_2 12%; SiO_2 37%). Even
359 accounting for the lower carbonate content, sample Cor13-21d has an Mg-richer composition
360 (MgO 11 wt.%) compared to metasomatic marbles.

361 Comparing the average composition of metasomatic marbles with Stage#1 diopside-
362 lawsonite rock (Table 1), the following features can be outlined. Despite the variability of the
363 protolith (with more or less abundant lawsonite), CaO is always enriched (CaO in
364 metasomatic marbles is about double that in Stage#1 rocks). MgO variations are more
365 difficult to evaluate, as they depend not only on the silicate content of metasomatic marbles,
366 but also on the initial diopside modal proportion of Stage#1 rock (cf. samples OF3598 and
367 COE5, Table 1). The reference calcschist (sample COR13-32) fits the range of compositions
368 of Alpine calcschists (Busigny et al. 2003, Galvez et al., 2013b). The reference ophicarbonate
369 sample (sample COR13-30a), has a Mg-rich composition (13 wt.% vs. 3 wt.% in metasomatic
370 marbles), similar to sample COR13-21d.

371 Whole-rock Rare-Earth Element (REE) analyses of most analyzed samples have
372 positive slopes ($La_N/Lu_N>1$) comparable to the reference calcschist and the host diopside-
373 lawsonite rock formed at the expense of carbonate free, continental basement
374 metasedimentary rocks (Fig. 6; Martin et al., 2011; Vitale Brovarone et al., 2014). Only
375 sample COR13-21d differs significantly. It has a rather flat REE pattern, except for a slight
376 negative Ce anomaly (Fig. 6). This pattern matches reasonably well with the ophicarbonate
377 standard and passive margin serpentinites (Barnes et al., 2014; Deschamps et al., 2013;
378 Kodolányi et al., 2011). This sample also has a significantly higher Ni and Cr content than the

379 other analyzed samples (1022 and 2114 ppm respectively, Table S2). These patterns suggest
380 an ultramafic signature for this sample.

381

382 **7. Carbon and oxygen stable isotope analysis of Ca-carbonate and clinopyroxene**

383 C and O isotopic compositions of calcite from metasomatic marbles (including veins) were
384 analyzes, as well as the O isotopic compositions of Stage#1 diopside and Stage#2 omphacite.
385 For reference, calcite from calcschist and ophicarbonate was also analyzed. Analyses of
386 carbon and oxygen isotopes of calcite are reported in Table S3.

387 For all samples (reference calcschists and ophicarbonate as well as metasomatic
388 marbles) calcite $\delta^{13}C$ values vary little and average 1.1‰ (±1.2, 1σ) (Fig. 7a), consistent with
389 marine sedimentary carbonate rocks (Plank and Langmuir, 1998). The average calcite $\delta^{18}O$
390 value of metasomatic marbles is 14.3‰ (±3.2, 1σ) (Fig. 7a). The two reference calcschists
391 (from ca. 8 to 50 m from the serpentinite, across strike) have an average $\delta^{18}O$ of 21.5‰ (±1.5,
392 1σ). The ophicarbonate analyzed in this study has $\delta^{18}O$ of 11‰. Carbonate in veins cutting
393 across carbonate-free, diopside-rich rocks has very low $\delta^{18}O$ 10.6‰ (±0.2, 1σ), independent
394 of vein distance from the serpentinite. Carbonate in samples collected from outcrops with
395 higher carbonate/silicate ratios (e.g. carbonate mode 70%) display more dispersed values that
396 vary from ~12 to ~18‰. In these rocks, samples collected a few centimeters from the
397 serpentinite body have an average value of ~14‰ (9 samples), whereas the two samples
398 collected far from the serpentinite (i.e. more than 3m) and within the analyzed interaction
399 zone (cf. Figs. 6 and S3 and Table S3 for sample location and respective REE patterns and
400 isotope composition) have a heavier signature of ~18‰. A simple correlation cannot be
401 established between the distance from the serpentinite and the $\delta^{18}O$ values within the reaction
402 zone. Indeed, Stage#2 omphacite-carbonate veins far from the serpentinite body (up to 8 m

403 from the contact) have low $\delta^{18}O$ values similar to metasomatic marble sampled a few cm from
404 the serpentinite body (e.g. samples 2COR14-4i and 1COR14-11a; Table S3). However, taken
405 as a whole, metasomatic marbles, overlying the serpentinite body, have lower $\delta^{18}O$ compared
406 to the reference calcschists. Indeed, calcschists that lack the petrographic characteristics of
407 intense fluid-rock interaction present in metasomatic marbles always have heavier values (ca.
408 21‰, see samples COR13-32 and 1COR12-11Q, Table S3), even if they crop out at less than
409 1m from the metasomatic zones.

410 Reconnaissance oxygen isotope measurements on silicate minerals were performed in
411 order to test for isotopic equilibrium between the two clinopyroxene generations (Stage#1
412 diopside and Stage#2 omphacite) and the vein infill carbonate. The analyzed sample is
413 composed of the host Stage#1 diopside-rich rock cut across by a Stage#2 calcite-omphacite
414 vein (Figs. 3d and S2). Diopside has $\delta^{18}O$ values of ~6‰. Vein infill omphacite has heavier
415 $\delta^{18}O$ of ~7‰. Fractionation factors available from literature data ($\Delta_{calcite\text{-}clinopyroxene}$ from
416 Hoffbauer et al., 1994, , Table S3.1), give equilibrium temperature of 494°C (±30°) for the
417 omphacite-carbonate assemblage and 426°C (±20°) for diopside-carbonate using the same
418 database. These differing temperatures are consistent with textural disequilibrium between the
419 mineral pairs (carbonate-diopside and diopside-omphacite). The omphacite-calcite
420 thermometer yields temperatures closer to the estimated peak T conditions of the
421 metamorphic unit (490-530°C, see Section 2). This observation suggests isotopic equilibrium
422 for the omphacite+carbonate paragenesis and confirms the microtextural observations (see
423 Section 5).

424 Equilibrium was likely reached by fluid-mediated reactions. However, this
425 interpretation must be taken with caution because only one sample was analyzed. The
426 composition of an aqueous fluid in equilibrium with these minerals was also calculated at 500
427 °C (i.e. near peak conditions). The $\delta^{18}O$ of a fluid in equilibrium with the measured Ca-

carbonate is 10.1‰ ($\Delta_{cal\text{-}H2O}$=0.62, Zheng et al. 1994). For the analyzed omphacite composition, the water $\delta^{18}O$ obtained is 8.4‰ ($\Delta_{di\text{-}H2O}$=-1.95, $\Delta_{ae\text{-}H2O}$=-0.07 and $\Delta_{jd\text{-}H2O}$=-0.14, Zheng et al., 1993). Although the fractionation factors for lawsonite are not available, the diopside-water equilibrium, can be used as a proxy for fluid in equilibrium with the Stage#1 assemblage implying that the fluid $\delta^{18}O$=8‰. The mismatch between calcite-water and omphacite-water oxygen composition equilibrium is quite small as well as for water in equilibrium with diopside. It is worth noting that the estimated fluid composition is similar for both metasomatic stages.

8. DISCUSSION

8.1 Fluid-mediated carbonation at high-pressure conditions

Detecting metasomatism in metasedimentary rocks is often challenging owing to the variability of protolith compositions (Bebout and Burton, 1989; Ague, 2003). The occurrence of carbonate in metasedimentary rock is common, and in most cases likely reflects the primary composition of the subducted rocks. However, the direct spatial association of Stage#2 metasomatic marbles along major fluid conduits characterized by intense metasomatism (Martin et al., 2011; Vitale Brovarone et al., 2014) suggests that the evolution of these rocks was mediated by the interaction with external fluids (e.g. Ague, 2003).

Rod-shaped calcite crystals in marbles from eclogite-facies terrains have been described in Syros (Greece) and the Sivrihisar belt (Turkey) (Brady et al., 2004; Seaton et al., 2009), and have been interpreted as topotactic pseudomorphs of calcite after aragonite. Both studies regard carbonate as a primary constituent of the rock and do not consider fluid-mediated precipitation. In the study case, we consider this hypothesis unlikely based on

several lines of evidence. Textures like crack-seal and networked carbonate veins cutting across carbonate-free metasomatic rocks suggest high pore fluid pressure and hydrofracturing (e.g. Bebout and Barton, 1989). This evidence clearly points to the percolation of carbonic fluids along lithological boundaries, and their precipitation of carbonate. As reported in Sections 2 and 5, field relations and microstructural features (Figs. 4) suggest carbonation of the Ca-Mg-rich silicate rocks. The lateral (along schistosity) transition from carbonate-free diopside-lawsonite rocks and metasomatic marbles is evidence for chemical interaction occurring between a carbonic fluid and the host-rock assemblage. Progressive replacement of diopside-rich rocks by carbonate is demonstrated at the microscale by the corroded texture of precursor minerals (embayed and atoll-like diopside, Figs. 4d, e and 5a) and producing coronas in contact with carbonates (e.g. omphacite rims on diopside, Figs. 5a and b). The carbonate isotopic composition presented in this work (Section 7) further supports the hypothesis of fluid-mediated carbonate precipitation. All metasomatic marbles are composed of Ca-carbonate (calcite after aragonite). This appears unlikely in the case of metamorphic recrystallization of rocks containing significant whole rock Mg (Table S2). These observations suggest that carbonate precipitation occurred via two concurrent processes of fluid-rock interaction: crack-sealing (carbonation by volume increase, Section 3) and mineral replacement (Section 5). Note that carbonation of mafic rocks during high-pressure metamorphism was also suggested by Boundy et al. (2002) for eclogite-facies rocks from the Lindås Nappe (Caledonides, Western Norway) and by Kleine et al. (2014) for blueschist-facies rocks from Syros. Both authors proposed carbonation of mafic eclogites along a shear zone affected by fluid circulation. Similarly, Nishiyama (1990) proposed metamorphic carbonation during exhumation of blueschist-facies metabasic rocks in association with serpentinites in the Nishisonogi metamorphic complex (Japan).

475 Based on these observations, the metasomatic history of the Corsican eclogite-facies marbles
476 can be subdivided into two stages, both occurring at high-pressure conditions during
477 subduction.

478 *Stage#1*: calcic metasomatism of protolith metasedimentary rocks or continental basement
479 transforms metasediments in contact with serpentinites to Ca-Mg rocks dominantly composed
480 of diopside and lawsonite during prograde metamorphism (cf. Martin et al., 2011; Vitale
481 Brovarone et al., 2014).

482 *Stage#2*: carbon-bearing fluid reacts with the pre-existing diopside-lawsonite rock and
483 associated serpentinites leading to the precipitation of carbonate-dominated assemblages as
484 either crack-filling material, or by replacing silicate minerals. The metamorphic conditions for
485 this stage are constrained to high-pressure conditions by the assemblage aragonite +
486 omphacite + lawsonite + garnet that characterize several of the analyzed samples ($P > 1.5$
487 GPa at 450-500 °C), and supported by the estimated O isotope Ca-carbonate-omphacite
488 equilibrium T of ca. 500 °C.

489 *8.2 Stable isotopes: marker of rock carbonation and fluid source?*

490 Stable isotope geochemistry has provided important information for the study of high-
491 pressure metasomatic processes involving carbonates (Valley 1986; Wang & Rumble 1999;
492 Ague and Nicolescu, 2014; Galvez et al., 2013a,b). The trends of decreasing $\delta^{13}C$ and $\delta^{18}O$
493 isotopic composition of the metamorphic carbonates may be attributed to: (i) inheritance of
494 protolith isotopic signatures (Wang and Rumble, 1999), (ii) carbonate-silicate isotopic
495 exchange; (iii) devolatilization reactions driven by increasing temperatures (Wang and
496 Rumble, 1999), or (iv) interaction with COH fluids (Ague and Nicolescu, 2014; Galvez et al.,
497 2013a,b).

498 In this study, hypothesis (i) can be ruled out by comparison of the isotopic signature of
499 metasomatic marbles with calcschists far from the metasomatic zones. The reference
500 calcschists have $\delta^{13}C$ values of ca. 0‰ and $\delta^{18}O$ of ca. 21‰ similar to those of calcschists and
501 carbonate veins (for similar metamorphic conditions) in Alpine Corsica (Cartwright and
502 Buick, 2000; Miller et al., 2001), Western Alps (Cartwright and Barnicoat, 1999; Cook-
503 Kollars et al., 2014), and Cyclades (Ague and Nicolescu, 2014) (Fig. 7a). The metasomatic
504 marble $\delta^{13}C$ values are shifted toward heavier values, although still overlapping the
505 compositional range of seawater carbonates, whereas $\delta^{18}O$ values display a much greater
506 dispersion towards lower values (Fig. 7a).

507 Partial silicate-carbonate oxygen isotope exchange (hypothesis ii) is an alternative way
508 to explain low $\delta^{18}O$ (with almost no change in $\delta^{13}C$). We discard this scenario for two
509 reasons. 1) At temperatures of 500°C, isotopic exchange by diffusion between two solid
510 phases is expected to be very slow and thus restricted to grain margins. 2) Even if interface-
511 coupled dissolution precipitation allowed faster isotopic exchange (Putnis and John, 2010),
512 the $\delta^{18}O$ achieved in the carbonate after such equilibration should be correlated with the
513 silicate content (the lowest $\delta^{18}O$ being observed for the highest silicate content; Wang and
514 Rumble 1999; Cook-Kollars et al. 2014). Figure 7b shows that no correlation exists between
515 the $\delta^{18}O$ of carbonate and the silicate content in the rock.

516 As a test for the third hypothesis, the metasomatic marbles are compared with
517 carbonates that have experienced devolatilization reactions. Carbonates in skarns formed by
518 contact metamorphism are characterized by a strong decrease of $\delta^{13}C$ coupled with a smaller
519 $\delta^{18}O$ decrease during decarbonation (e.g. Valley 1986). The trend observed in Corsican
520 metasomatic marbles of $\delta^{18}O$ decreasing with $\delta^{13}C$ remaining constant is actually different
521 from a devolatilization trend (Fig. 7c).

Considering the compelling evidences for fluid-rock interactions and metasomatism, interactions between rocks and COH fluids (hypothesis iv) is considered the most likely hypothesis. Galvez et al. (2013b) reported carbonate reduction to graphite in contact with serpentinites in the high-pressure units of Alpine Corsica. In this study, carbonates display a peculiar variation showing a decreasing $\delta^{18}O$ coupled with increasing $\delta^{13}C$. Residual carbonate in samples affected by carbonate dissolution driven by serpentinite-derived fluids described by Ague and Nicolescu (2014) show a drop in oxygen isotopic signature compared to the protolith (6 to 10‰ lower values). However, changes in $\delta^{13}C$ are very small, with only a 1.5‰ decrease. Both carbonate precipitation and dissolution seem to be characterized by a large decrease in $\delta^{18}O$ and little to no change in $\delta^{13}C$ (Fig. 7c; cf. Section 8.3 for additional discussion). The $\delta^{13}C$ values of metasomatic marbles are similar to those typical of carbonates in marine sediments (e.g. Hoefs, 2013) and subducted oceanic suites ($\delta^{13}C$ close to 0‰; e.g. Miller et al., 2001), thus indicating that carbon in the fluids derives from marine carbonates, likely from the overlying carbonate-bearing metasedimentary rocks. The low $\delta^{18}O$ values rather point to fluids equilibrated with silicates in mafic or ultramafic rocks, possibly including Stage#1 metasomatic rocks (Miller et al., 2001; Martin et al., 2014; Vitale Brovarone et al., 2014; Angiboust et al., 2014). The large serpentinite body in contact with the rocks of this study would represent a plausible source for aqueous fluid with a light oxygen signature. Despite the lack of evidence for serpentinite dehydration (e.g. metamorphic olivine) in the samples from Alpine Corsica, a growing number of studies (Faccenda 2014; Wilson et al., 2014) have proposed that fluids generated at depth can move up along the plate interface and interact with shallower slab-forming rocks. Ague and Nicolescu (2014) proposed that fluid equilibrated with mafic and ultramafic rocks can drive stoichiometric carbonate dissolution, resulting in aqueous fluid enriched in carbon with $\delta^{13}C$ around 0‰. However, if fluids were diluted, the contribution of oxygen from dissolved carbonates to the

547 oxygen isotopic signature of the fluid is expected to be very low. The preservation of
548 lawsonite requires very low X_{CO2} fluid concentrations (X_{CO2}<0.005; e.g. Nitsh, 1972),
549 demonstrating that the carbon-bearing fluid was dominantly aqueous. Altogether, these
550 considerations point to metasomatic marbles formation by interaction with aqueous fluids
551 bringing isotopic signatures of both dissolved carbonates and mafic/ultramafic reservoirs.

552

553 *8.3 Rock carbonation during subduction: implications for the deep carbon cycle*

554 The behavior of carbonate, more specifically Ca-carbonate, during subduction has long been a
555 matter of debate. Few experimental studies of Ca-carbonate solubility in H_2O have been
556 conducted at P-T conditions appropriate for subduction metamorphism (Walther and Long,
557 1986; Fein and Walther, 1989; Newton and Manning, 2002; Caciagli and Manning, 2003;
558 Manning et al., 2013; Facq et al., 2014). Caciagli and Manning (2003) showed that calcite
559 solubility increases with P and T at high-pressure conditions. Ca-carbonate dissolution at
560 high-pressure conditions has been demonstrated to be very efficient in natural environments
561 (P > ~2 GPa, Frezzotti et al., 2011; Ague and Nicolescu, 2014), and it is now considered as a
562 major process for the mobilization of carbon in subduction zones (Kelemen & Manning,
563 2015). Carbonic fluids produced by carbonate dissolution are thus a potential source of
564 carbon for carbonate precipitation in subduction zones. Figure 8a shows a rough carbon
565 fluxes mass balance (see Section 4.3 for method of carbon fluxes calculation) considering
566 carbon bound by rock carbonation in metasomatic marbles vs. the amount of carbon dioxide
567 released by dissolution and devolatilization reactions estimated in previous field-based studies
568 in analog geological settings (Ague and Nicolescu, 2014; Cook-Kollars et al., 2014). The
569 amount of CO_2 released by decarbonation (green and orange bars) is small compared to that
570 released by dissolution (blue bar). Consequently, processes related to carbonate solubility

mobilize carbon in greater quantities than simple decarbonation reactions (Ague and Nicolescu, 2014). A possible explanation for this result is that devolatilization reactions are controlled and limited by the presence of silicate phases with which the carbonate minerals can react, regardless of the fluid fluxes. The red bar in the diagram indicates the inferred amount of CO_2 transferred from the fluid to the rock by rock carbonation, considering an initial carbon content of 0 g per 100g of precursor rock. The amount of carbon bound per 100g of rock is directly comparable with that released by carbonate dissolution. This observation suggests that a large amount of dissolved carbon can be re-bound into the solid phase by rock carbonation, and that carbonate dissolution and rock carbonation at high-pressure conditions are both crucial processes controlling carbon fluxes during subduction.

Slab-parallel ascent of fluids may represent a suitable configuration to enhance the efficiency of rock-carbonation reactions, if favorable conditions occur (Lazar et al., 2014; Kelemen and Manning, 2015; Sverjensky et al., 2014). Figure 8b shows the Ca-carbonate solubility in aqueous fluid as a function of P and T (after Kelemen & Manning 2015) along with the predicted P-T path for cold subduction (after Syracuse et al., 2010). Deep metamorphic fluids ascending parallel to the downgoing slab would cut across the solubility curves during their ascent. Although prediction of fluid slab-parallel ascent by numerical modeling is still limited (e.g. Faccenda, 2014; Wilson et al., 2014), natural samples from high-pressure (this study) and ultrahigh-pressure exhumed metamorphic terrains may preserve records of the interactions of deep-fluids with the slab-forming rocks. In this study, it is shown how major lithological interfaces (e.g. crust-metasediments) may represent ideal settings for fluid channelization. In addition, the data presented here also show that Ca-Mg-rich rocks (diopside-rich) and ultramafic rocks are reactive lithologies for rock carbonation at high-pressure conditions.

595 Interaction between slab-derived fluids and mantle-wedge rocks also represents a
596 possible lithological configuration for rock carbonation. High amounts of carbonic fluids
597 resulting from slab carbonate dissolution are expected to percolate through the mantle wedge,
598 where ultramafic rocks may represent a suitable reactant (Kelemen and Manning 2015).
599 Based on the current knowledge of processes occurring along the plate interface (e.g.
600 Syracuse et al., 2010), carbonation of the hydrated mantle wedge overlying subducting slabs
601 seems unlikely in the case of vertical upward migration (rising T), whereas it is more
602 plausible along the slab-mantle interface (decreasing T). Exhumation of cold serpentinite
603 diapirs in forearc settings may also be a possible environment for rock carbonation (Fryer,
604 1992). Future studies on rocks ascribed to the mantle wedge are needed to test this hypothesis.

605 **9. Conclusions**

606 The petrological and geochemical results of this study indicate that the Corsican eclogite-
607 facies marbles found along major fluid conduits have a metasomatic origin and were formed
608 at high-pressure conditions during subduction. These rocks formed by carbonation of Ca-Mg
609 silicate rocks by percolating carbonic fluids (Fig. 9). This implies that carbonic fluids formed
610 during prograde carbonate dissolution may not be directly and fully transferred to the mantle
611 wedge, but can also flow along slab interfaces (i.e. crust-metasediments) and reprecipitate
612 carbonates under favorable conditions in both slab- and mantle-forming rocks. Carbonates
613 precipitating from these fluids then display a characteristic geochemical and isotopic
614 signature. Therefore, carbonation of Ca-Mg silicate rocks at high-pressure-low temperature
615 conditions can be an efficient process to lock carbon in the rock, as is well documented at
616 shallow and seafloor conditions (Guyot et al., 2011; Matter and Kelemen, 2009). The
617 widespread occurrence of these rocks in the units of Alpine Corsica is likely a consequence of
618 the overall exceptional preservation of pristine high-pressure-low temperature assemblages in
619 this belt. This suggests that analogous rocks and processes may have occurred in more

retrogressed high-pressure belts, such as the Western Alps, the Cyclades and Turkey, and may be happening today in present-day subduction zones as well.

Whether or not high-pressure rock carbonation permanently binds carbon in the rock cannot be easily established at present. For example, high-pressure carbonated rocks can experience successive carbonate dissolution in deeper parts of subduction zones. Nonetheless, carbonation of slab- and mantle-forming rocks (Fig. 9) likely modulates the residence time of carbon in different reservoirs, and can modify the oxygen and carbon isotopic signature of carbonates in subduction zones. Considering a longer time-scale perspective (e.g. time elapsed from subduction initiation to continental collision), carbonation at high-pressure conditions may ultimately influence the fluctuation of CO_2 emissions at volcanic arcs during the life of a subduction zone, and thereby the fluctuation of atmospheric CO_2 over geological time scales (e.g. Berner & Kothavala, 2001).

Acknowledgment: The research leading to these results has received funding from the Deep Carbon Observatory, the University Pierre et Marie Curie (Paris 6) and Sorbonne Universités. Imène Esteve and Sébastien Charron are thanked for their technical support in the SEM platform. Benoit Baptiste is thanked for his technical support in the XRD platform. Scanning Electron Microscope (SEM) facility of the Institut de Mineralogie, Physique des Materiaux et Cosmochimie is supported by Région Ile de France grant SESAME 2006 N_ I-07-593/R, INSU-CNRS, INP-CNRS, University Pierre et Marie Curie – Paris 6, and by the French National Research Agency (ANR) grant no. ANR-07-BLAN-0124-01. Michel Fialin and Nicolas Rividi (CAMPARIS service) are thanked for their technical support during EMPA measurement.

References

Ague, J.J., 2003. Fluid Infiltration and Transport of Major, Minor, and Trace Elements During Regional Metamorphism of Carbonate Rocks, Wepawaug Schist, Connecticut, USA. American Journal of Science 303, 753–816. doi:10.2475/ajs.303.9.753

Ague, J.J., Nicolescu, S., 2014. Carbon dioxide released from subduction zones by fluid-mediated reactions. Nature Geosci 7, 355–360.

650 Alt, J.C., Teagle, D.A.H., 1999. The uptake of carbon during alteration of ocean crust. Geochimica et
651 Cosmochimica Acta 63, 1527–1535. doi:10.1016/S0016-7037(99)00123-4
652 Angiboust, S., Pettke, T., De Hoog, J.C.M., Caron, B., Oncken, O., 2014. Channelized Fluid Flow and Eclogite-
653 facies Metasomatism along the Subduction Shear Zone. Journal of Petrology 55, 883–916.
654 doi:10.1093/petrology/egu010
655 Bach, W., Rosner, M., Jöns, N., Rausch, S., Robinson, L.F., Paulick, H., Erzinger, J., 2011. Carbonate veins
656 trace seawater circulation during exhumation and uplift of mantle rock: Results from ODP Leg 209.
657 Earth and Planetary Science Letters 311, 242–252. doi:10.1016/j.epsl.2011.09.021
658 Barnes, J.D., Beltrando, M., Lee, C.-T.A., Cisneros, M., Loewy, S., Chin, E., 2014. Geochemistry of Alpine
659 serpentinites from rifting to subduction: A view across paleogeographic domains and metamorphic
660 grade. Chemical Geology 389, 29–47. doi:10.1016/j.chemgeo.2014.09.012
661 Bebout, G.E., Barton, M.D., 1989. Fluid flow and metasomatism in a subduction zone hydrothermal system:
662 Catalina Schist terrane, California. Geology 17, 976–980.
663 Beltrando, M., Manatschal, G., Mohn, G., Dal Piaz, G.V., Vitale Brovarone, A., Masini, E., 2014. Recognizing
664 remnants of magma-poor rifted margins in high-pressure orogenic belts: The Alpine case study. Earth-
665 Science Reviews 131, 88–115. doi:10.1016/j.earscirev.2014.01.001
666 Berner, R.A., Kothavala, Z., 2001. GEOCARB III: a revised model of atmospheric CO2 over Phanerozoic time.
667 American Journal of Science 301, 182–204.
668 Boundy, T.M., Donohue, C.L., Essene, E.J., Mezger, K., Austrheim, H., 2002. Discovery of eclogite facies
669 carbonate rocks from the Lind\a as Nappe, Caledonides, Western Norway. Journal of Metamorphic
670 Geology 20, 649–667.
671 Bowman, J.R., Valley, J.W., Kita, N.T., 2009. Mechanisms of oxygen isotopic exchange and isotopic evolution
672 of 18O/16O-depleted periclase zone marbles in the Alta aureole, Utah: insights from ion microprobe
673 analysis of calcite. Contributions to Mineralogy and Petrology 157, 77–93. doi:10.1007/s00410-008-
674 0321-1
675 Brady, J.B., Markley, M.J., Schumacher, J.C., Cheney, J.T., Bianciardi, G.A., 2004. Aragonite pseudomorphs in
676 high-pressure marbles of Syros, Greece. Journal of Structural Geology 26, 3–9. doi:10.1016/S0191-
677 8141(03)00099-3
678 Caciagli, N.C., Manning, C.E., 2003. The solubility of calcite in water at 6-16kbar and 500-800°C. Contributions
679 to Mineralogy and Petrology 146, 275–285. doi:10.1007/s00410-003-0501-y
680 Cartwright, I., Barnicoat, C.A., 1999. Stable isotope geochemistry of Alpine ophiolites: a window to ocean-floor
681 hydrothermal alteration and constraints on fluid–rock interaction during high-pressure metamorphism.
682 International Journal of Earth Sciences 88, 219–235. doi:10.1007/s005310050261
683 Cartwright, I., Buick, I.S., 2000. Fluid generation, vein formation and the degree of fluid–rock interaction during
684 decompression of high-pressure terranes: the Schistes Lustrés, Alpine Corsica, France. Journal of
685 Metamorphic Geology 18, 607–624.
686 Connolly, J.A.D., 2005. Computation of phase equilibria by linear programming: A tool for geodynamic
687 modeling and its application to subduction zone decarbonation. Earth and Planetary Science Letters
688 236, 524–541. doi:10.1016/j.epsl.2005.04.033
689 Cook-Kollars, J., Bebout, G.E., Collins, N.C., Angiboust, S., Agard, P., 2014. Subduction zone metamorphic
690 pathway for deep carbon cycling: I. Evidence from HP/UHP metasedimentary rocks, Italian Alps.
691 Chemical Geology 386, 31–48. doi:10.1016/j.chemgeo.2014.07.013
692 Deschamps, F., Godard, M., Guillot, S., Hattori, K., 2013. Geochemistry of subduction zone serpentinites: A
693 review. Lithos 178, 96–127. doi:10.1016/j.lithos.2013.05.019
694 Faccenda, M., 2014. Water in the slab: A trilogy. Tectonophysics 614, 1–30. doi:10.1016/j.tecto.2013.12.020
695 Facq, S., Daniel, I., Montagnac, G., Cardon, H., Sverjensky, D.A., 2014. In situ Raman study and
696 thermodynamic model of aqueous carbonate speciation in equilibrium with aragonite under subduction
697 zone conditions. Geochimica et Cosmochimica Acta 132, 375–390. doi:10.1016/j.gca.2014.01.030
698 Fein, J., Walther, J., 1989. Calcite solubility and speciation in supercritical NaCl-HCl aqueous fluids. Contr.
699 Mineral. and Petrol. 103, 317–324. doi:10.1007/BF00402918
700 Fournier M., Jolivet, L., Goff, B., Dubois, R., 1991. Alpine Corsica metamorphic core complex. Tectonics 10,
701 1173–1186
702 Frezzotti, M.L., Selverstone, J., Sharp, Z.D., Compagnoni, R., 2011. Carbonate dissolution during subduction
703 revealed by diamond-bearing rocks from the Alps. Nature Geoscience 4, 703–706.
704 doi:10.1038/ngeo1246
705 Fryer, P., Pearce, J.A., Stokking, L.B., others, 1992. 36. A synthesis of Leg 125 drilling of serpentine seamounts
706 on the Mariana and Izu–Bonin forearcs, in: Proceedings of the Ocean Drilling Program, Scientific
707 Results. pp. 593–614.

Galvez, M.E., Beyssac, O., Martinez, I., Benzerara, K., Chaduteau, C., Malvoisin, B., Malavieille, J., 2013a. Graphite formation by carbonate reduction during subduction. Nature Geoscience 6, 473–477. doi:10.1038/ngeo1827

Galvez, M.E., Martinez, I., Beyssac, O., Benzerara, K., Agrinier, P., Assayag, N., 2013b. Metasomatism and graphite formation at a lithological interface in Malaspina (Alpine Corsica, France). Contributions to Mineralogy and Petrology 166, 1687–1708. doi:10.1007/s00410-013-0949-3

Gerdes, M.L., Baumgartner, L.P., Person, M., Rumble, D., 1995. One-and two-dimensional models of fluid flow and stable isotope exchange at an outcrop in the Adamello contact aureole, Southern Alps, Italy. American Mineralogist 80, 1004–1019.

Gerdes, M.L., Baumgartner, L.P., Valley, J.W., 1999. Stable isotopic evidence for limited fluid flow through dolomitic marble in the Adamello contact aureole, Cima Uzza, Italy. Journal of Petrology 40, 853–872.

Gorman, P.J., Kerrick, D.M., Connolly, J.A.D., 2006. Modeling open system metamorphic decarbonation of subducting slabs: METAMORPHIC DECARBONATION. Geochemistry, Geophysics, Geosystems 7, n/a–n/a. doi:10.1029/2005GC001125

Guyot, F., Daval, D., Dupraz, S., Martinez, I., Ménez, B., Sissmann, O., 2011. CO2 geological storage: The environmental mineralogy perspective. Comptes Rendus Geoscience 343, 246–259. doi:10.1016/j.crte.2010.12.007

Hoefs, J., 2013. Stable isotope geochemistry. Springer Science & Business Media.

Hoffbauer, R., Hoernes, S., Fiorentini, E., 1994. Oxygen isotope thermometry based on a refined increment method and its application to granulite-grade rocks from Sri Lanka. Precambrian Research 66, 199–220. doi:10.1016/0301-9268(94)90051-5

Jébrak, M., 1997. Hydrothermal breccias in vein-type ore deposits: A review of mechanisms, morphology and size distribution. Ore Geology Reviews 12, 111–134. doi:10.1016/S0169-1368(97)00009-7

Jolivet, L., Daniel, J.-M., Fournier, M., 1991. Geometry and kinematics of extension in Alpine Corsica. Earth and Planetary Science Letters 104, 278–291. doi:10.1016/0012-821X(91)90209-Z

Jolivet, L., Dubois, R., Fournier, M., Goffé, B., Michard, A., Jourdan, C., 1990. Ductile extension in alpine Corsica. Geology 18, 1007–1010. doi:10.1130/0091-7613(1990)018<1007:DEIAC>2.3.CO;2

Kelemen, P.B., Manning, C.E., 2015. Reevaluating carbon fluxes in subduction zones, what goes down, mostly comes up. Proceedings of the National Academy of Sciences 201507889. doi:10.1073/pnas.1507889112

Kerrick, D.M., Connolly, J.A.D., 2001. Metamorphic devolatilization of subducted marine sediments and the transport of volatiles into the Earth's mantle. Nature 411, 293–296.

Kleine, B.I., Skelton, A.D.L., Huet, B., Pitcairn, I.K., 2014. Preservation of Blueschist-facies Minerals along a Shear Zone by Coupled Metasomatism and Fast-flowing CO2-bearing Fluids. Journal of Petrology 55, 1905–1939. doi:10.1093/petrology/egu045

Kodolanyi, J., Pettke, T., Spandler, C., Kamber, B.S., Gmeling, K., 2012. Geochemistry of Ocean Floor and Fore-arc Serpentinites: Constraints on the Ultramafic Input to Subduction Zones. Journal of Petrology 53, 235–270. doi:10.1093/petrology/egr058

Lazar, C., Zhang, C., Manning, C.E., Mysen, B.O., 2014. Redox effects on calcite-portlandite-fluid equilibria at forearc conditions: Carbon mobility, methanogenesis, and reduction melting of calcite. American Mineralogist 99, 1604–1615. doi:10.2138/am.2014.4696

Malavieille, Chemenda, Larroque, 1998. Evolutionary model for Alpine Corsica: mechanism for ophiolite emplacement and exhumation of high-pressure rocks. Terra Nova 10, 317–322. doi:10.1046/j.1365-3121.1998.00208.x

Malvoisin, B., Chopin, C., Brunet, F., Galvez, M.E., 2012. Low-temperature Wollastonite Formed by Carbonate Reduction: a Marker of Serpentinite Redox Conditions. Journal of Petrology 53, 159–176. doi:10.1093/petrology/egr060

Manning, C.E., Shock, E.L., Sverjensky, D.A., 2013. The Chemistry of Carbon in Aqueous Fluids at Crustal and Upper-Mantle Conditions: Experimental and Theoretical Constraints. Reviews in Mineralogy and Geochemistry 75, 109–148. doi:10.2138/rmg.2013.75.5

Martin, L.A.J., Rubatto, D., Crépisson, C., Hermann, J., Putlitz, B., Vitale-Brovarone, A., 2014. Garnet oxygen analysis by SHRIMP-SI: Matrix corrections and application to high-pressure metasomatic rocks from Alpine Corsica. Chemical Geology 374-375, 25–36. doi:10.1016/j.chemgeo.2014.02.010

Martin, L.A.J., Rubatto, D., Vitale Brovarone, A., Hermann, J., 2011. Late Eocene lawsonite-eclogite facies metasomatism of a granulite sliver associated to ophiolites in Alpine Corsica. Lithos 125, 620–640. doi:10.1016/j.lithos.2011.03.015

Matter, J.M., Kelemen, P.B., 2009. Permanent storage of carbon dioxide in geological reservoirs by mineral carbonation. Nature Geosci 2, 837–841. doi:10.1038/ngeo683

McCrea, J.M., 1950. On the Isotopic Chemistry of Carbonates and a Paleotemperature Scale. The Journal of Chemical Physics 18, 849. doi:10.1063/1.1747785

Miller, J.A., Cartwright, I., Buick, I.S., Barnicoat, A.C., 2001. An O-isotope profile through the HP–LT Corsican ophiolite, France and its implications for fluid flow during subduction. Chemical Geology 178, 43–69.

Molina, J.F., Poli, S., 2000. Carbonate stability and fluid composition in subducted oceanic crust: an experimental study on H2O–CO2-bearing basalts. Earth and Planetary Science Letters 176, 295–310. doi:10.1016/S0012-821X(00)00021-2

Molli, G., Malavieille, J., 2011. Orogenic processes and the Corsica/Apennines geodynamic evolution: insights from Taiwan. Int J Earth Sci (Geol Rundsch) 100, 1207–1224. doi:10.1007/s00531-010-0598-y

Morimoto, N., 1988. Nomenclature of Pyroxenes. Mineralogy and Petrology 39, 55–76. doi:10.1007/BF01226262

Newton, R.C., Manning, C.E., 2002. Experimental determination of calcite solubility in H2O-NaCl solutions at deep crust/upper mantle pressures and temperatures: Implications for metasomatic processes in shear zones. American Mineralogist 87, 1401–1409.

Nishiyama, T., 1990. CO2-metasomatism of a metabasite block in a serpentine melange from the Nishisonogi metamorphic rocks, southwest Japan. Contributions to Mineralogy and Petrology 104, 35–46.

Nitsch, K.-H., 1972. The P-T-X_{CO2} Stabilitätsfeld von Lawsonit. Contributions to Mineralogy and Petrology 34, 116–134. doi:10.1007/BF00373768

Poli, S., 2015. Carbon mobilized at shallow depths in subduction zones by carbonatitic liquids. Nature Geoscience 8, 633–636. doi:10.1038/ngeo2464.

Poli, S., Franzolin, E., Fumagalli, P., Crottini, A., 2009. The transport of carbon and hydrogen in subducted oceanic crust: An experimental study to 5 GPa. Earth and Planetary Science Letters 278, 350–360. doi:10.1016/j.epsl.2008.12.022

Putnis, A., John, T., 2010. Replacement Processes in the Earth's Crust. Elements 6, 159–164. doi:10.2113/gselements.6.3.159

Ravna, E.J.K., Andersen, T.B., Jolivet, L., De Capitani, C., 2010. Cold subduction and the formation of lawsonite eclogite – constraints from prograde evolution of eclogitized pillow lava from Corsica. Journal of Metamorphic Geology 28, 381–395. doi:10.1111/j.1525-1314.2010.00870.x

Rumble III, D., Farquhar, J., Young, E.D., Christensen, C.P., 1997. In situ oxygen isotope analysis with an excimer laser using F2 and BrF5 reagents and O2 gas as analyte. Geochimica et Cosmochimica Acta 61, 4229–4234. doi:10.1016/S0016-7037(97)00232-9

Seaton, N.C.A., Whitney, D.L., Teyssier, C., Toraman, E., Heizler, M.T., 2009. Recrystallization of high-pressure marble (Sivrihisar, Turkey). Tectonophysics 479, 241–253. doi:10.1016/j.tecto.2009.08.015

Sun, S., McDonough, W.F., 1989. Chemical and isotopic systematics of oceanic basalts: implications for mantle composition and processes. Geological Society, London, Special Publications 42, 313–345. doi:10.1144/GSL.SP.1989.042.01.19

Sverjensky, D.A., Stagno, V., Huang, F., 2014. Important role for organic carbon in subduction-zone fluids in the deep carbon cycle. Nature Geoscience 7, 909–913. doi:10.1038/ngeo2291

Syracuse, E.M., van Keken, P.E., Abers, G.A., 2010. The global range of subduction zone thermal models. Physics of the Earth and Planetary Interiors 183, 73–90. doi:10.1016/j.pepi.2010.02.004

Valley, J.W., 1986. Stable isotope geochemistry of metamorphic rocks. Reviews in Mineralogy and Geochemistry 16, 445–489.

Vitale Brovarone, A., Alard, O., Beyssac, O., Martin, L., Picatto, M., 2014. Lawsonite metasomatism and trace element recycling in subduction zones. Journal of Metamorphic Geology 32, 489–514. doi:10.1111/jmg.12074

Vitale Brovarone, A., Beltrando, M., Malavieille, J., Giuntoli, F., Tondella, E., Groppo, C., Beyssac, O., Compagnoni, R., 2011b. Inherited Ocean–Continent Transition zones in deeply subducted terranes: Insights from Alpine Corsica. Lithos 124, 273–290. doi:10.1016/j.lithos.2011.02.013

Vitale Brovarone, A., Beyssac, O., 2014. Lawsonite metasomatism: A new route for water to the deep Earth. Earth and Planetary Science Letters 393, 275–284. doi:10.1016/j.epsl.2014.03.001

Vitale Brovarone, A., Beyssac, O., Malavieille, J., Molli, G., Beltrando, M., Compagnoni, R., 2013. Stacking and metamorphism of continuous segments of subducted lithosphere in a high-pressure wedge: The example of Alpine Corsica (France). Earth-Science Reviews 116, 35–56. doi:10.1016/j.earscirev.2012.10.003

Vitale Brovarone, A., Groppo, C., HetéNyi, G., Compagnoni, R., Malavieille, J., 2011a. Coexistence of lawsonite-bearing eclogite and blueschist: phase equilibria modelling of Alpine Corsica metabasalts and petrological evolution of subducting slabs. Journal of Metamorphic Geology 29, 583–600. doi:10.1111/j.1525-1314.2011.00931.x

Vitale Brovarone, A., Herwartz, D., 2013. Timing of HP metamorphism in the Schistes Lustrés of Alpine Corsica: New Lu–Hf garnet and lawsonite ages. Lithos 172-173, 175–191. doi:10.1016/j.lithos.2013.03.009

827 Wang, Q., Rumble, D., 1999. Oxygen and carbon isotope composition from the UHP Shuanghe marbles, Dabie
828 Mountains, China. Science in China Series D: Earth Sciences 42, 88–96.
829 Wilson, C.R., Spiegelman, M., van Keken, P.E., Hacker, B.R., 2014. Fluid flow in subduction zones: The role of
830 solid rheology and compaction pressure. Earth and Planetary Science Letters 401, 261–274.
831 doi:10.1016/j.epsl.2014.05.052

Figure Captions

Fig.1: Geological background of the study area. a) Simplified regional setting of Alpine Corsica (France) in the Western Mediterranean region. Modified after Molli and Malavieille (2011). b) Simplified tectono-stratigraphic map of Alpine Corsica. The black box indicates the position of the study area. c) Simplified geological map of the San Petrone unit. Figures modified after Vitale Brovarone et al. (2013).

Fig. 2: simplified structural sketch summarizing the field relationships between the different rock types and the location of the study samples. The star refers to metasomatic marbles formed at the expense of former serpentinites.

Fig. 3: Representative textural features of metasomatic marble in the field. a) Crack-seal texture in a metasomatic marble lens located in the metasomatic rind formed along the continental basement-serpentinite contact. Dashed lines mark the schistosity in the host rock and the orientation of the remains of the host rock in the carbonate-rich domain (see detail in b). Note that the silicate layers are deflected toward the carbonate vein. b) Detail of carbonate layers containing rod-shaped aragonite pseudomorphs alternating with vein-parallel bands of wallrock inclusions. c) Interdigitation of rod-shape carbonate with Stage#1 diopside-lawsonite rock. d) Carbonate+omphacite vein cutting across Stage#1 diopside+lawsonite rock. The black dotted line marks the vein wall and the green area overdrawn marks the selvage extension. e) and f) Photograph and related interpretative sketch of a hydraulic breccia (types defined by Jébrak 1997) consisting of angular clasts of diopside+lawsonite rock (Stage#1 metasomatism) sealed by a network of veins containing rod-shaped carbonate crystals. g and h) Outcrop with high carbonate/silicate ratio and corresponding sketch. Rounded chunks of Stage#1 diopside-lawsonite rock float in a carbonate matrix. Microtextures in the carbonate-rich domains suggest digestion and chemical replacement of Stage#1 silicates by carbonate. Di=diospide; Lws=lawsonite.

Fig. 4: Progressive transformation of a precursor Stage#1 carbonate-free, diopside-lawsonite rock into a Stage#2 metasomatic marble. a) Stage#2 metasomatic marble cropping out along the serpentinite-metasediment contact. The marble (grey) is interdigitated with the host Stage#1 diopside-lawsonite rock (green). The foliation of the diopsode-lawsonite rock (dashed line) can be followed in the carbonate layer. b) Thin section scan showing the interdigitation texture of silicate and carbonate layers analogous to that documented at the outcrop scale in part (a). Different degrees of carbonation are observed. White boxes indicate the location of the photomicrographs c, d and e. c) Plane polarized light photomicrograph and corresponding sketch of the preserved portion of the metasomatic diopside + lawsonite protolith; fan-shape diopside and lawsonite crystals statically crystallized. d) Plane polarized light photomicrograph and corresponding sketch of the patchy distribution of carbonate pods that characterizes a partially carbonated domain. Here, Stage#1 diopside aggregates are cut by the carbonate and some fragments are preserved as relicts in carbonate layers. e) Plane polarized light photomicrograph and corresponding sketch of a highly carbonated portion. Here the rock is transformed into a metasomatic marble; prismatic carbonate crystals are well developed. A few remnants of Stage#1 diopside are preserved; these relicts display embayed rims and atoll-like textures. In every sketch, Stage#1 diopside + lawsonite domains are represented in green, whereas rod-shaped carbonate is in light beige.

Fig. 5: Backscattered electron (BSE) images obtained by SEM depicting micro scale textural relationships resulting from fluid-rock interaction. a) BSE image of atoll-like Stage#1 diopside suggesting a digestion of a silicate clast by carbonate; the Stage#1 diopsidic core is dissolved in favor of carbonate while a Stage#2 Na-Al rich rim (omphacite) crystallized in textural equilibrium with the carbonate. Small fragments of diopside are preserved as inclusions in carbonate crystals (red lines). b) BSE image of wallrock selvage shown in Figure 3d. Diopside is overgrown by omphacite rim. Omphacite rims have the same composition as the vein infill omphacite crystals (Table S1). c) Plane polarized light photomicrograph of diopside with aegirine-augite rim in sample COR13-21d. Cal=calcite, Omp=omphacite, Di=diopside; Agt=aegirine-augite, Act=actinolite.

Fig. 6: Whole-rock chondrite normalized REE patterns (CI values from Sun and McDonough, 1989) for metasomatic marbles (orange lines, see Fig. S3 for details), reference calcschist and ophicarbonate (solid and dashed black lines, respectively), and Stage#1 diopside + lawsonite metasomatic rock (solid green line). The shaded field represents the range of passive margin serpentinite whole-rock compositions (either actual or metamorphic equivalent of Tethyan ocean floor; data from Barnes et al., 2014; Kodolányi et al., 2012).

Fig. 7: Carbon and Oxygen stable isotopic analyses of calcite. a) Calcite $\delta^{13}C$ vs. $\delta^{18}O$ plot of metasomatic marbles (this study), blueschist and eclogite-facies marbles and calcite veins from other studies (Ague and Nicolescu, 2014; Cartwright and Buick, 2000; Cook-Kollars et al., 2014; Galvez et al., 2013b). Only data for non-metasomatic calcschists in Ague and Nicolescu (2014) and Galvez et al. (2013b) are reported. b) The rock silicate mineral content vs. calcite $\delta^{18}O$ values. The dispersion of data illustrates the lack of correlation between the light O isotopic signature and the silicate content. Analyses of reference calcschists and ophicarbonate are also reported. We plotted data for samples that were also analyzed for their bulk rock composition (samples COR13-32; COR13-30a; COR13-21b; COR13-21d; COR13-27e; COR13-17c; COR13-22c; COR13-28c; Table S3). c) Metasomatic marble and reference calcschists $\delta^{18}O$ vs. $\delta^{13}C$ plot. Shaded areas correspond to geochemical trend of carbonate affected by devolatilization (Bowman et al., 2009; Gerdes et al., 1995, 1999), and carbonate reduction (Galvez et al., 2013b). Isotopic composition of carbonates affected by carbonate dissolution is also reported (blue diamonds, Ague and Nicolescu, 2014).

Fig. 8: Carbon fluxes during subduction metamorphism. a) Bar diagram reporting the estimation of grams of CO_2 release per 100 g of precursor rock during carbonate dissolution (Ague and Nicolescu 2014, blue bar) and decarbonation reactions (Cook-Kollars et al., 2014, calculation by Perple_X software and natural sample estimation, green and orange bars respectively) and grams of CO_2 bound per 100 g of precursor rock via carbonate precipitation (red bar, this study). b) Contours of [C] in parts per million for aqueous fluid saturated in $CaCO_3$ as a function of P and T. The red arrow indicates the P-T path of Alpine Corsica (Vitale Brovarone et al., 2011a). The star corresponds to the $\Delta_{cal\text{-}omp}$ equilibrium temperature. The green field represents the predicted P-T path for active subduction (D80 model, Syracuse et al., 2010). Figure adapted from Kelemen & Manning (2015).

Fig. 9: Schematic illustration showing the percolation of COH fluids parallel to the subducting slab. The decreasing T and consequent decrease in carbonate solubility along this ascent path together with the interaction

with slab or mantle rock is a suitable context for carbonate precipitation via vein injection and mineral carbonation.

Table 1: Whole rock major element composition of metasomatic marble, Stage#1 diopside+lawsonite rock (OF3598) and Stage#1 rock with lawsonite>70% (COE5)

Fig. S1: Raman spectrum of aragonite inclusion in garnet.

Fig. S2: picture showing a detail of an omphacite-calcite vein. Omphacite grows from the vein wall toward the center.

Fig. S3: Whole-rock chondrite normalized REE patterns (CI values from Sun and McDonough, 1989) for metasomatic marbles, reference calcschist and ophicarbonate (solid and dashed black lines, respectively), and Stage#1 diopside + lawsonite metasomatic rock (dashed blue line). The shaded field represents the range of passive margin serpentinite whole-rock compositions (either actual or metamorphic equivalent of Tethyan ocean floor; data from Barnes et al., 2014; Kodolányi et al., 2012).

Table S1: Representative clinopyroxene analyses.

Table S2: Whole rock composition of analyzed samples (major and selected trace elements). Analyses below the lower detection limit are labeled "<d.l.". Values in wt.%.

Table S3: Stable isotopes analyses of calcite. Analyses made in duplicate.

Table S3.1: Stable oxygen isotopes analyses of clinopyroxenes, average value of calcite filling vein and calculated equilibrium T.

Table S4: Representative garnet analyses.

Table S5: Representative amphibole, lawsonite, phengite, pumpellyite analyses.

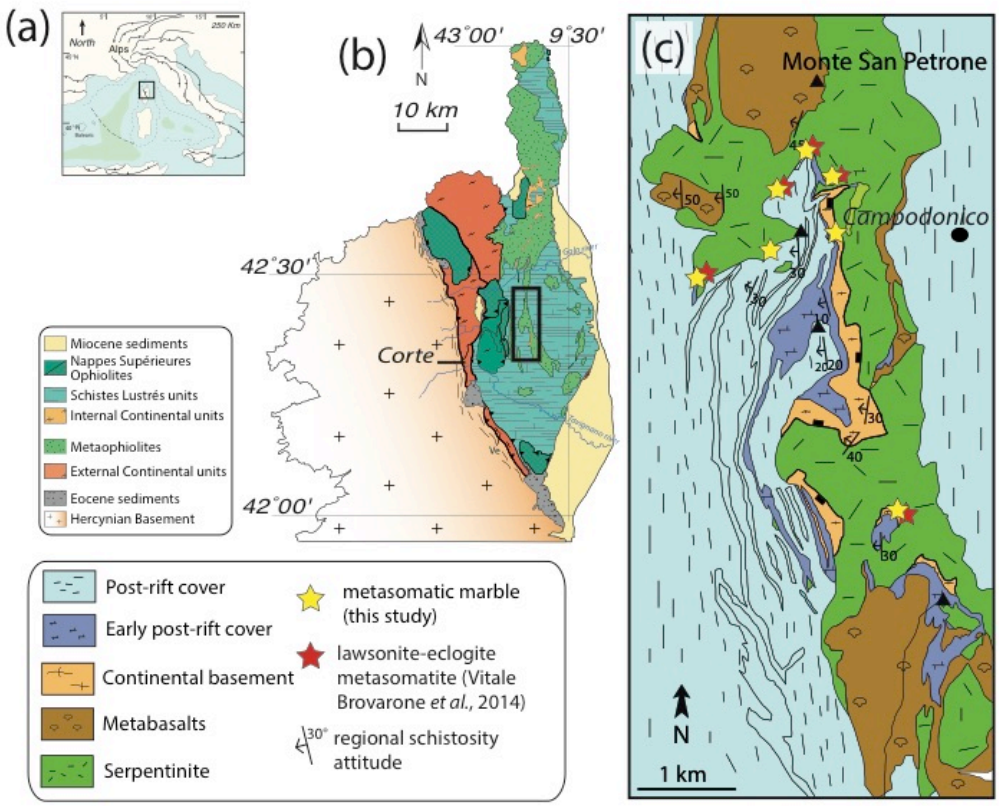

934 **Fig. 1**

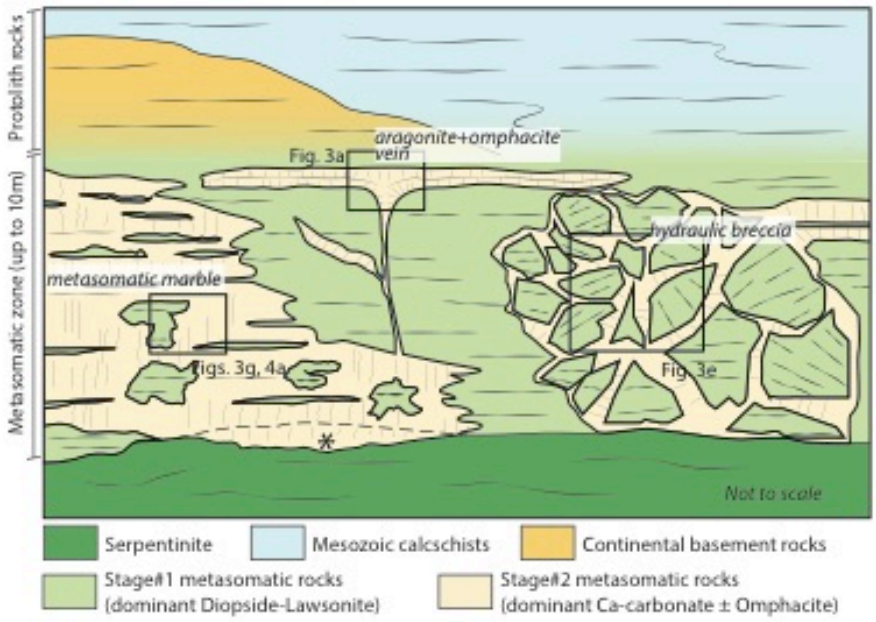

935 **Fig. 2**

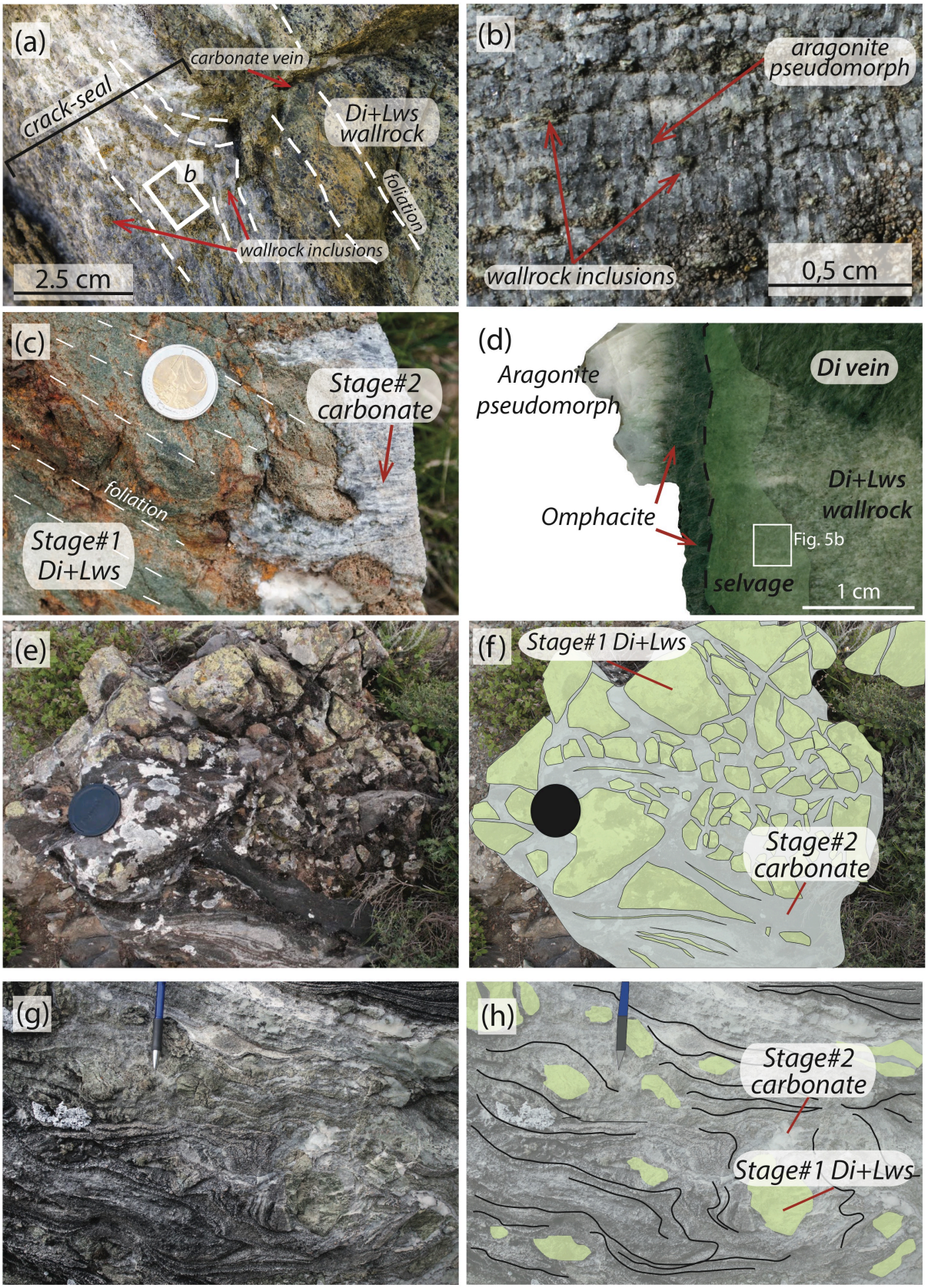
(a)
carbonate vein
crack-seal
Di+Lws
wallrock
b
foliation
wallrock inclusions
2.5 cm
(b)
aragonite
pseudomorph
wallrock inclusions
0,5 cm
(c)
Stage#2
carbonate
foliation
Stage#1
Di+Lws
(d)
Aragonite
pseudomorph
Di vein
Di+Lws
wallrock
Omphacite
Fig. 5b
selvage
1 cm
(e)
(f)
Stage#1 Di+Lws
Stage#2
carbonate
(g)
(h)
Stage#2
carbonate
Stage#1 Di+Lws

936 **Fig. 3**

937

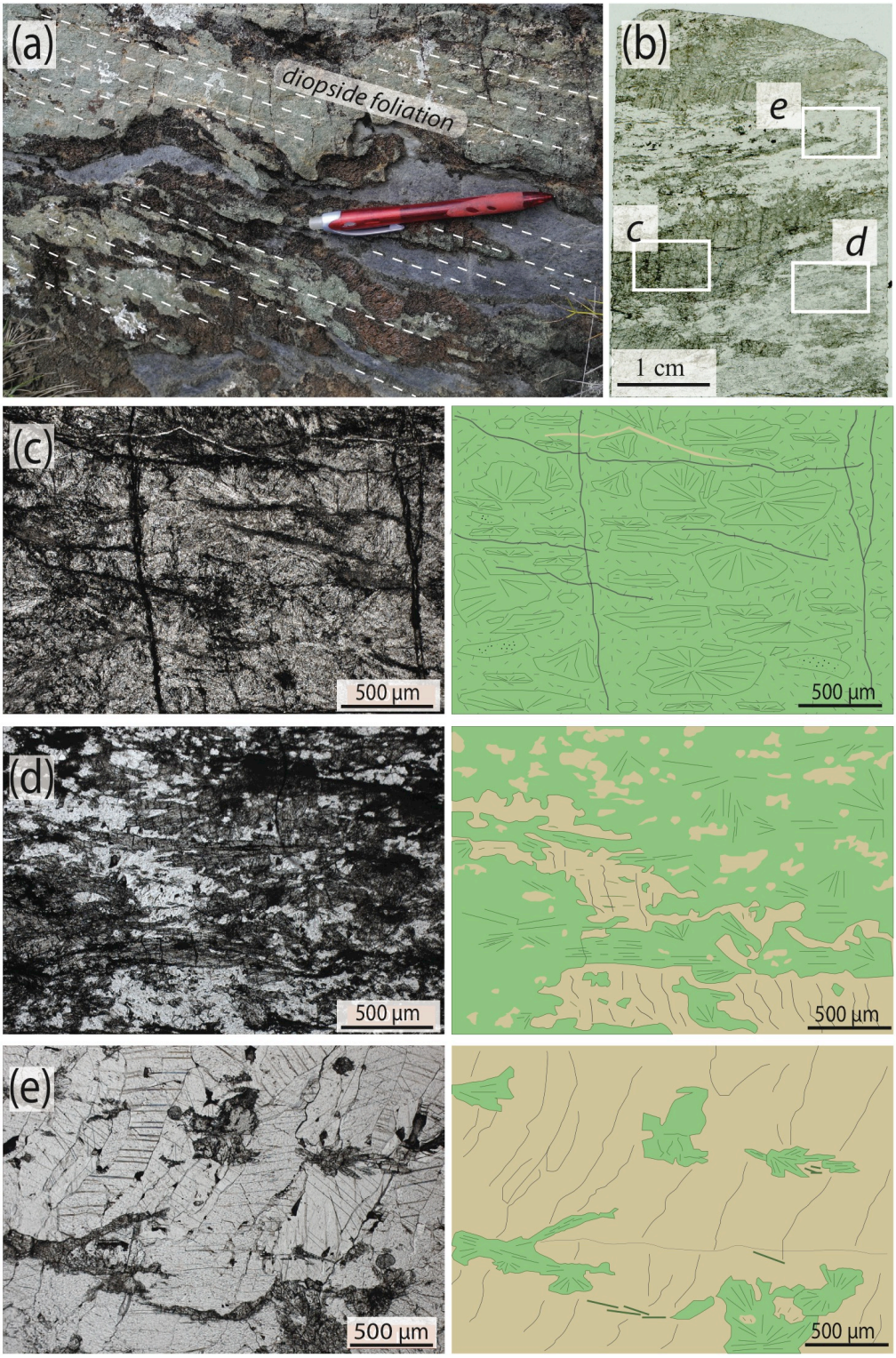

938 **Fig. 4**

939

940

941

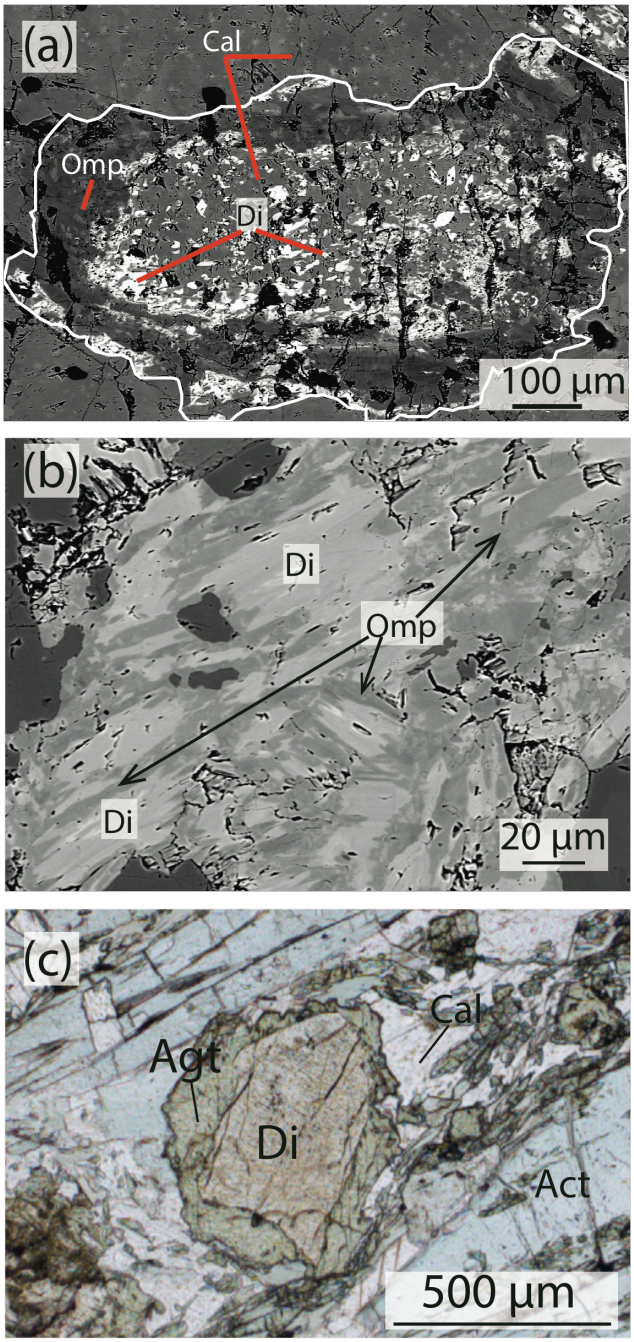

942

943 **Fig. 5**

944

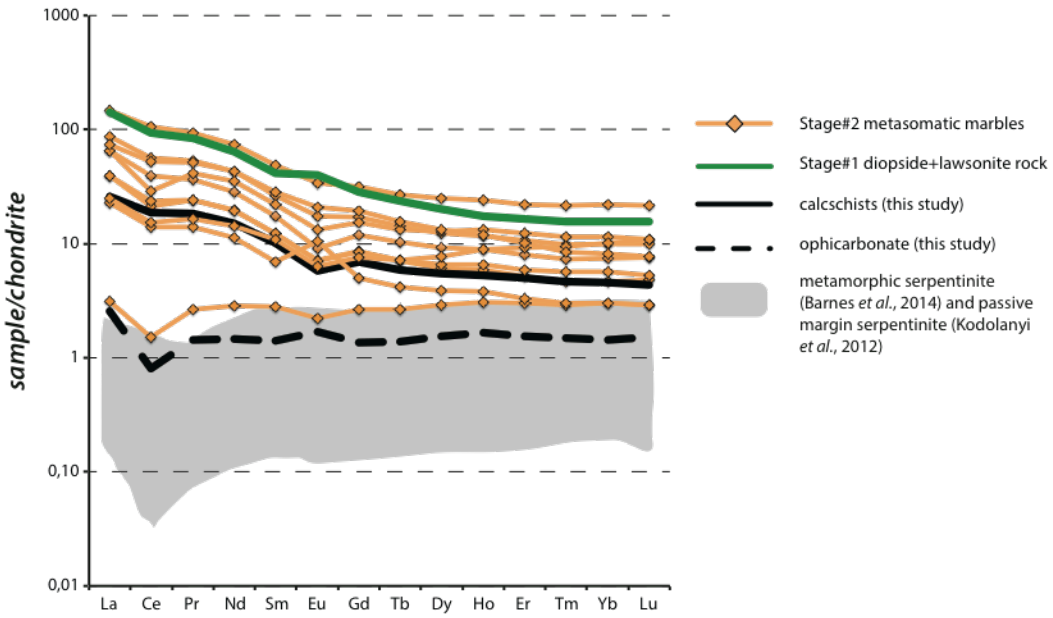

945 **Fig. 6**

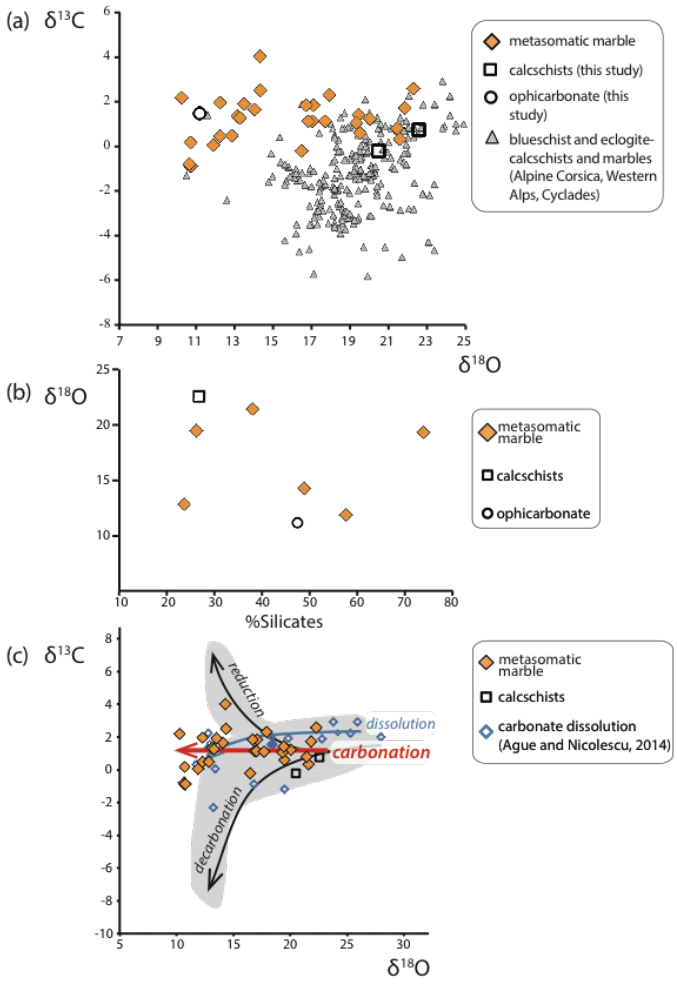

946 **Fig. 7**

947

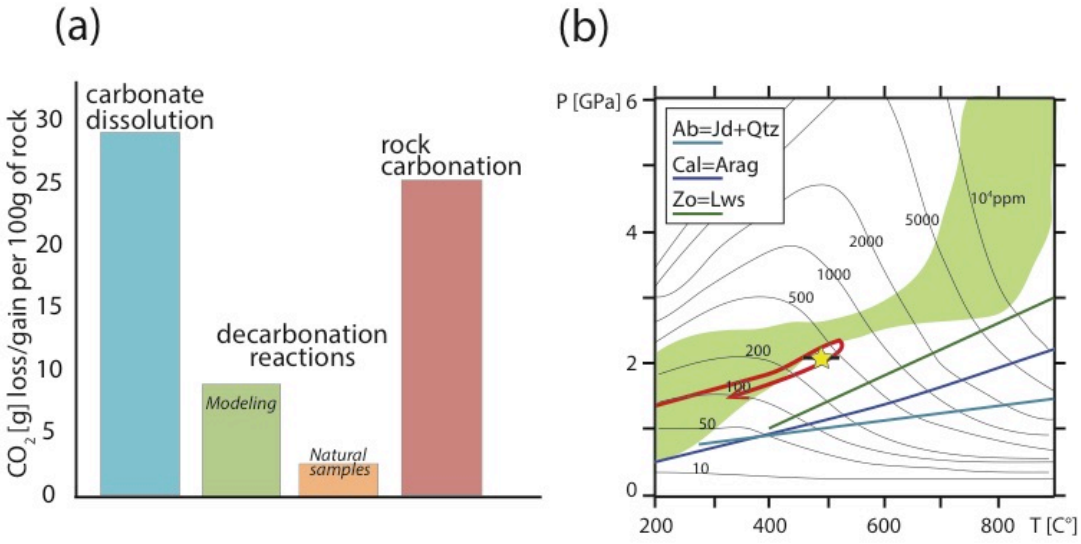

948 **Fig. 8**

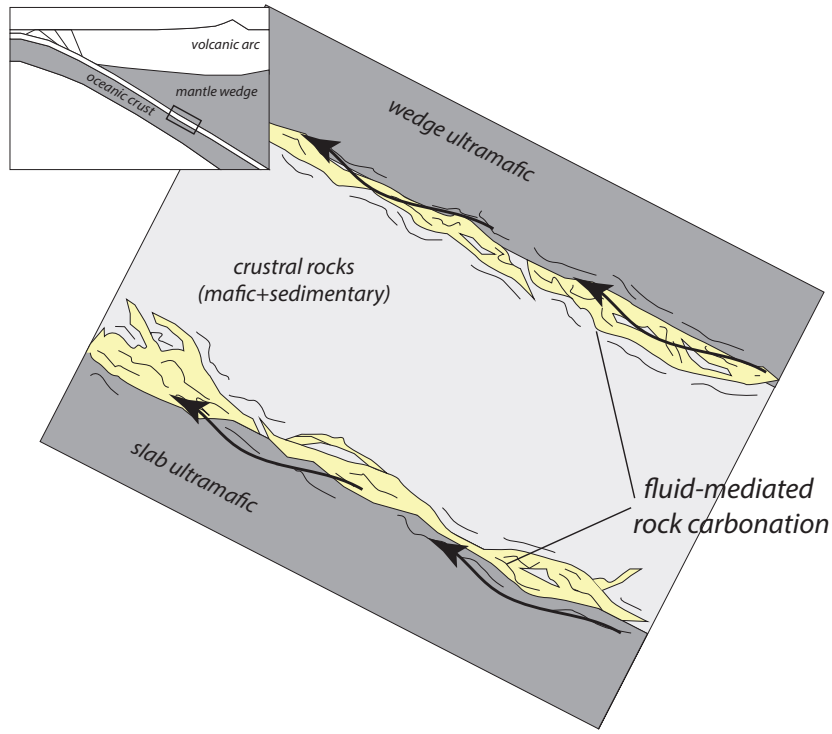

949 **Fig. 9**

Table 1: whole rock major element composition for metasomatic marbles (see Table S2 for details), Stage#1 diopside-lawsonite rock (OF3598) and Stage#1 rock with lawsonite>70% (COE5).

Sample	Metasomatic marble (n=4)	1σ	OF3598[a]	COE5[b]
			Stage#1 rock	
SiO2	20.44	5.65	45.30	40.6
Al2O3	4.97	2.94	15.11	25.6
Fe2O3	3.22	1.14	5.03	2.28
MnO	0.18	0.16	0.11	0.13
MgO	3.14	1.77	6.95	1.8
CaO	39.23	5.32	20.62	17.65
Na2O	0.92	0.95	0.47	0.51
K2O	0.12	0.16	0.01	0.24
TiO2	0.18	0.11	0.65	1.94
P2O5	0.09	0.04	0.11	0.41
LOI	27.05	5.12	5.57	7.94
Tot	99.54		99.94	99.10

[a]from Vitale Brovarone et al., 2014
[b]from Martin et al., 2011

950